JBUON 2013; 18(3): 788-794
ISSN: 1107-0625, online ISSN: 2241-6293 • www.jbuon.com
E-mail: editorial_office@jbuon.com

ORIGINAL ARTICLE

Magnetic resonance imaging and image analysis of post - radiation changes of bone marrow in patients with skeletal metastases

O. Romanos, E. Solomou, P. Georgiadis, D. Kardamakis, D. Siablis

University Hospital of Patras, Department of Clinical Radiology, MRI Unit, Rion – Patras, Greece

Summary

Purpose: *To evaluate the post-radiation lesions of the bone marrow with magnetic resonance imaging (MRI) and image analysis in patients with bone metastases undergoing radiation therapy (RT).*

Methods: *Thirty-five patients with bone metastases were studied from June 2008 to December 2010. All patients had osseous metastases from various primary malignancies and underwent palliative RT. MRI was performed in a Philips Gyroscan Intera 1T scanner at the beginning of RT and 12 -18 days later. T1-TSE, T2-TSE and short tau inversion recovery (STIR) sequences were used. All images obtained were evaluated for early post-radiation lesions. Additionally, 1st and 2nd order textural features were extracted from these images and were introduced into a probabilistic neural network (PNN) classifier in order to create an automated classification system for those lesions.*

Results: *Changes of signal intensity in T1-TSE, T2-TSE and STIR sequences were evaluated for the presence of edema, fatty conversion of the bone marrow or areas of hemorrhage within the limits of the irradiated area. The automated classification system showed positive results in correctly discriminating the post-radiation lesions that MRI revealed. The overall classification accuracy for discriminating between pre-radiation and post-radiation lesions was 93.2%. Furthermore, the overall classification accuracy for discriminating between post-radiation lesions was 86.67%.*

Conclusion: *It seems that MRI can evaluate the degree of early therapy-induced bone marrow lesions observed during the first 18 days from the beginning of RT. The proposed neural network-based classification system might be used as an assisting tool for the characterization of these lesions.*

Key words: *bone marrow, bone metastasis, image analysis, MRI, radiation therapy*

Introduction

The skeletal system is the 3rd commonest site for localization of metastasis after liver and lung. Nearly 70% of patients with cancer will develop bone metastases sometime, where most of them will be under palliative RT [1,2]

RT as a sole treatment modality

For many decades, RT has been established successfully as a treatment method for the management of metastatic bone disease [3], offering considerable pain relief and a reduction in complication rates [4,5]. This is valid for both single-fraction (SF) and multi-fraction (MF) RT, since the achieved overall pain response rates (partial and complete pain responses) are 58% and 59% respectively [4]. In addition, complete pain response (zero pain score) rates are 23% and 24% for SF and MF RT, respectively [4]. In cases of widespread metastatic skeletal disease, whole- or hemi-body RT offers substantial symptomatic pain relief in 91% of patients, with 45% experiencing a complete pain response [6].

Regarding the duration of pain relief by RT, in the pivotal trial conducted by the Radiation Therapy Oncology Group, a complete pain response has been recorded in 54% of patients with a median duration of 12 weeks, and at least a partial response in 90% of patients [7,8].

Correspondence to: Ekaterini Solomou, MD, PhD. University Hospital of Patras, Department of Clinical Radiology, MRI Unit, 26504, Rion – Patras, Greece. Tel: + 30 2610 999422, Fax: +30 2610 993988, E-mail: solomoua@upatras.gr
Received: 03/12/2012; Accepted: 28/12/2012

The exact mechanism of action by which pain relief is achieved through RT is uncertain. RT destroys a large percentage of tumor cells, even in cases of relatively radio-resistant tumors [9]. This causes shrinkage of the metastatic tumor mass, which may subsequently allow osteoblasts to repair and re-ossify metastatic skeletal lesions [10]. The tumor shrinkage by itself cannot though explain the early pain response that is observed within 24 to 48 hours post whole body RT in up to 25% of patients [11]. Moreover, it has been shown that RT suppresses urinary bone resorption markers, the level of suppression correlating with response to treatment. This fact may implicate that the analgesic effect of RT is achieved through an indirect inhibition of osteoclastic activity that results from the drastic decrease in the release of osteoclastic mediators from tumor cells at sites of metastatic bone lesions [12,13]. This could be an important link for the possible synergistic activity with bisphosphonates (BPs).

MRI is the method of choice to detect not only skeletal metastases, but also to evaluate post-radiation changes in the bone marrow, as it provides information at the level of cellular and chemical composition. MRI findings have been extensively investigated by many authors to assess early and late treatment related changes [14-18].

A definite time frame of bone marrow changes after low dose irradiation has not been specified so far. Up to date, there are many references in the literature concerning the post-radiation changes with MRI within and besides the fields of the irradiated area [19-21], but to our knowledge none of them involves post-radiation changes and image analysis classification systems.

Table 1. Summary of patients undergoing radiation therapy

Primary malignancy	*Number of patients*	*%*
Breast Ca	9	25.71
Prostate Ca	7	20
Lung Ca	7	20
Other malignancies*	12	34.29

*hepatocellular Ca (n=2), colorectal Ca (n=2), gastric Ca (n=2), melanoma (n=2), renal cell Ca (n=2), urinary bladder Ca (n=1), cervix Ca (n=1)

We focused on the early post-radiation bone marrow changes that occur within the irradiated area. The purpose of this study was to introduce an original automated classification system and evaluate its accuracy in the recognition and characterization of post-radiation bone marrow lesions that are detected with conventional MRI.

Methods

Clinical material

Thirty-five patients (23 male –12 female, age range 39-80 years, mean 64.9 years) with bone metastases were studied with MRI between June 2008 and December 2010. Inclusion criteria were (a) histologically confirmed solid tumors (obtained during surgery or CT-guided biopsy) and (b) bone metastases, confirmed by X-ray, CT, MRI, or bone scintigraphy. None of the patients had known blood or hematopoietic disease which could affect bone marrow characteristics. Patients with a history of pathologic fracture, epidural spinal cord

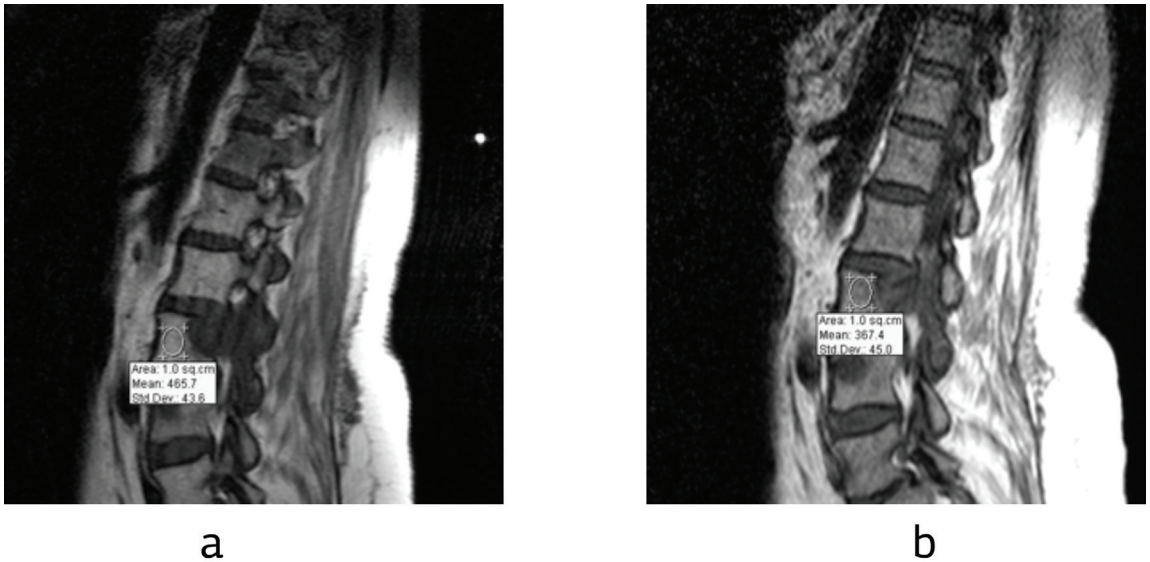

Figure 1. T1-SE images in a patient presented with metastases in the lumbar spine. (**a**) Before RT and (**b**) 18 days after the beginning of RT.

compression, hypercalcemia, hypocalcemia, Paget's disease, primary hyperparathyroidism, or patients with previous RT to the affected region were excluded.

All patients presented with osseous metastases in the spine or in the hips, except one patient who showed metastasis in the femoral bone. Metastases were originated from various primary malignancies (Table 1).

All patients received external-beam RT with a 6-MV linear accelerator to the specified treatment site. The total tumor dose delivered ranged from 30 to 40 Gy, with a daily dose of 1.8 –2.0 Gy. Patients received RT 5 days per week with a total treatment duration of 3–4.5 weeks.

Use of analgesics during the study fulfilled the World Health Organization criteria for pain relief. The study protocol was approved by the hospital's review committee. Written informed consent was obtained from all patients.

MRI was performed in a Philips Gyroscan Intera 1T scanner at the beginning of RT and 12 -18 days later (Figure 1). Coil of the thoracic or lumbar spine or body coils were used, depending on the metastatic site.

T1-TSE (TE/TR 627/12ms), T2-TSE (TE/TR 2710/120ms) and STIR sequences (TR/TI/TE 1824/70/90ms) were used in transverse and sagittal planes before gadolinium administration and fat suppression weighted images (SPIR) after gadolinium enhancement (TR/TE 905/12ms). Imaging parameters included matrix size 256x256, field of view (FOV) 400 mm and slice thickness 4 mm (intersection gap 0.4 mm).

These images were evaluated for early post-radiation lesions, according to the literature [15-22].

Qualitative evaluation

Visual evaluation was performed independently by two radiologists (E.S and O.R), who were not blinded to patient history, radiation dose or clinical data. They visually compared T1, T2 and STIR-weighted images before and during RT, in each patient. The presence of low signal on T1-TSE and high signal on T2-TSE and STIR images was considered as edema. The fatty displacement of bone marrow was estimated as high signal on T1-TSE and T2-TSE and low on STIR images. MR signals due to the presence of focal areas of hemorrhage were variable, due to the time of the examination [15-22].

Quantitative evaluation

Areas of interest were selected and measurements were evaluated by the method of Region of Interest (ROI). Elliptic areas of 1cm^2 were used on each vertebra. Each measurement was repeated 3 times for the intra-observer variation analysis as well as the calculation of the mean values. We avoided measurements near the cortex, the disc or veins, which could lead in false results [23].

Multiseries classification validation

Additionally, 1st and 2nd order textural features were extracted from these images and were introduced into a PNN classifier in order to create an automated classification system for those lesions.

Region of interest extraction and feature calculation

Utilizing these images, square ROIs were specified within the lesion area. From each ROI, a series of 36 features were extracted; 4 features from the ROI's histogram, expressing information concerning the frequency of appearance of each gray level; 22 from the co-occurrence matrices [24], reflecting the frequency of appearance of each gray level at adjacent pixels; and 10 from the run-length matrices [25], describing the frequency of appearance of a set of consecutive pixels having the same gray value (Table 2).

All features were normalized to zero mean and unit standard deviation [26], according to the equation (1):

$$x_i' = \frac{x_i - m}{std}$$

where x_i and x_i' are the i-th feature values before and after the normalization respectively, and m and std are the mean value and standard deviation, respectively, of feature x_i over all patterns and all classes.

Least squares feature transformation – probabilistic neural network classifier (LSFT-PNN)

Due to the small size of the dataset utilized in the present study, the PNN classifier was chosen. PNN is a non-parametric feed-forward neural network classifier that encompasses both the Bayes' classification approach and the Parzen's estimators of probability density functions [27]. The decision function of the PNN

Table 2. Textural features extracted

Methods	*Features*
Histogram (1st order statistics)	Mean Value, Standard Deviation, Skewness, Kurtosis
Mean and range of 0°, 45°, 90° and 135° co-occurrence matrices (2nd order statistics)	Angular Second Moment, Contrast, Correlation, Sum Of Squares, Inverse Difference Moment, Sum Average, Sum Variance, Sum Entropy, Entropy, Difference Variance, Difference Entropy
Mean and range of 0°, 45°, 90° and 135° run-length matrices (2nd order statistics)	Short Run Emphasis, Long Run Emphasis, Gray Level Non Uniformity, Run Length Non Uniformity, Run Percentage

classifier is described by the equation (2):

$$d_k(x) = \frac{1}{(2\pi)^{\frac{n}{2}}\sigma^n N_k}\sum_{i=1}^{N_k} e^{-\frac{\|x-x_i\|^2}{2\sigma^2}}$$

where x_i is the i_{th} training input pattern, x is the unknown pattern to be classified, N_k is the number of patterns forming the class x_k, n is the number of textural features forming the input pattern while sigma σ is an adjusting parameter, taking values ranging between 0 and 1. Training patterns x_i, prior to entering the PNN classifier, were transformed by means of a non-lineal least squares feature transformation (LSFT) technique, to render classes more separable by clustering the patterns of each class around arbitrary pre-selected points. The utilized LSFT method is an extension of the linear least squares mapping technique, introduced by Ahmed and Rao [28].

Classification scheme design

Two LSFT-PNN based classification systems were designed to discriminate between (a) pre-radiation and post-radiation lesions and (b) between the post-radiation lesions (oedema, fatty conversion and hemorrhage) (Figure 2).

The External-Cross-Validation (ECV) technique was used to avoid bias conditions [29], which may occur by using the same dataset in the feature selection and evaluation stages.

To combine the diagnostic information encapsulated in the MR images acquired with all three MR series (T1-TSE, T2-TSE and STIR), a multi-series classification procedure was utilized (Figure 3).

Accordingly, each ROI from each MR series was classified in a separate LSFT-PNN classifier. Finally, the output of each classifier was used in the formulation of a collective decision using the majority vote rule [26]. Thus, the output of the system was expressed as in equation (3):

$$\sum_{i=1}^{r} D_{ji} = \max_{k=1}\sum_{i=1}^{r} D_{ki}$$

where r is the number of classifiers and D_j is a binary decision value for the j^{th} class.

Results

Changes of signal intensity in T1-TSE, T2-TSE and STIR were evaluated for the presence of oedema, fatty conversion of the bone marrow and hemorrhage, within the limits of the irradiated area.

The best overall classification accuracy of the system designed to discriminate between pre-ra-

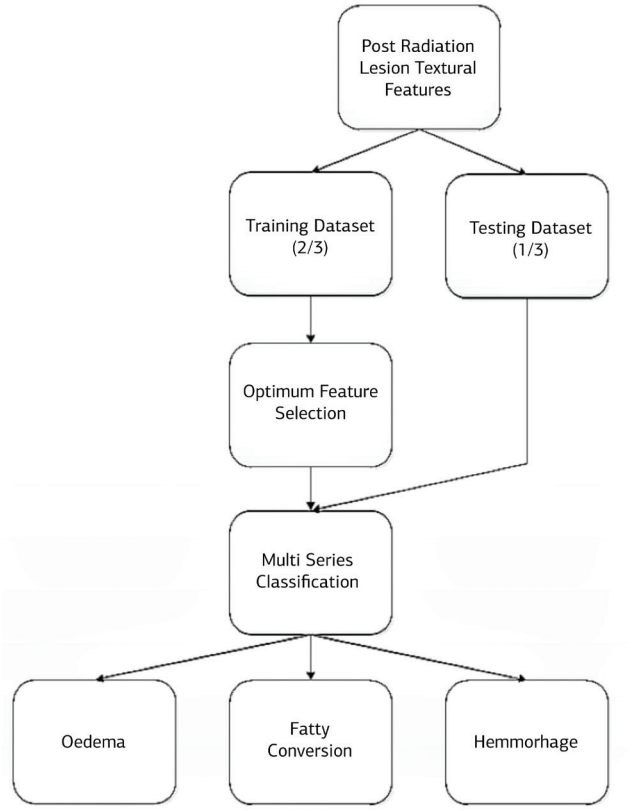

Figure 2. Classification system designed to discriminate between post-radiation lesions.

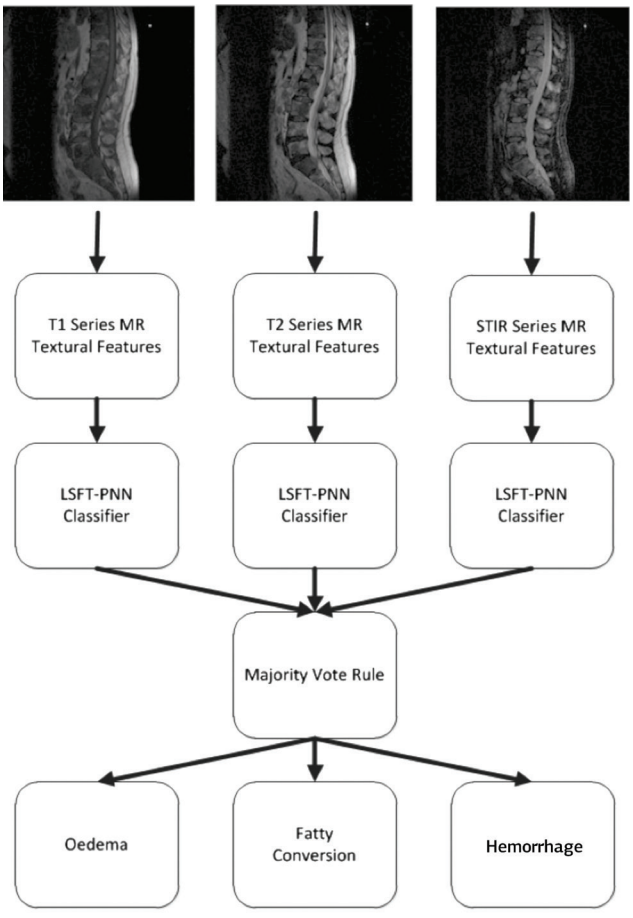

Figure 3. Multiseries classification procedure.

Table 3. Classification results utilizing the ECV method and the LSFT-PNN multi-sequence classification scheme (average after 10 ECV repetitions)

Number of features	*Pre-radiation vs post-radiation Overall accuracy (%)*	*Oedema vs fatty conversion vs hemorrhage Overall accuracy (%)*
1	51.16	33.33
2	74.42	46.67
3	88.37	63.33
4	93.02	76.67
5	76.07	86.67

diation and post-radiation lesions was 93.02% employing the LSFT-PNN multi-sequence classification scheme and the ECV method (Table 3).

Individual accuracies in discriminating between pre-radiation and post-radiation lesions were 90.91% and 95.24%, respectively.

Best feature vector, used for the optimal design of the classification scheme, comprised four textural features: the skewness, the difference entropy, the sum average and the sum entropy.

Employing the LSFT-PNN multi-sequence classification scheme and the ECV technique, the discrimination accuracy of the classification system designed to distinguish between the three types of post-radiation lesions (edema, fatty conversion and hemorrhage) was 86.67% (Table 3).

The best feature vector employed for the optimal design of the classification scheme, comprised five textural features: the standard deviation, the difference entropy, the sum average, the entropy and the long run emphasis.

Discussion

The role of MRI as a method of choice for the early detection and characterization of bone marrow post-therapeutic changes has been well established [30].

T1 and T2 relaxation times reflect the relative amounts of red marrow, yellow marrow and trabecular bone. The distribution of these components can be altered by several conditions, including infiltrating diseases and RT [17].

A variety of changes in irradiated osseous structures has been previously described in the literature, depending on the time intervals [19,31].

The effect of RT on bone marrow has been documented by histologic and gross anatomic studies. These studies have shown that shortly after the start of RT the bone marrow becomes hypocellular, its vascular architecture gets destructed and fatty marrow progressively replaces the hematopoietic marrow [32-34].

Because of these alterations, high signal intensity is produced in T1-TSE images. During the first weeks after the initiation of RT, areas of increased signal intensity in STIR images may represent edema, hemorrhage or an early reflux of non irradiated cells.

There has been controversy over the exact time when edema, hemorrhage and fatty degeneration appear and disappear [16,17,35].

In this study, we focused on these early post-radiation effects on the bone marrow. We used the information provided by conventional MRI in combination with an automated classification system in order to improve the detection and characterization of bone marrow alterations.

Onu et al. [36] documented that simple visual assessment of such processes has relatively low sensitivity. Quantitative assessment is considered as a better approach and has been used in several studies [36-38].

The classification system designed and used gave us the opportunity to determine and characterize precisely even the smallest lesions in the bone marrow which are not really obvious by other radiological methods. Our main aim was to improve the accuracy of the method in detecting early post-radiation alterations, as well as to further specify the time frame of these changes after low dose irradiation of the bone marrow.

It is very important to choose the most sensitive MR sequences for the detection even of the smallest alterations of the marrow. Previous studies have used either T1 or T2 weighted images to investigate these changes [30]. In our study, we combined all T1-TSE, before and after the use of paramagnetic contrast injection, as well as T2-TSE and STIR images, in order to get the maximum information in a reasonable examination time, according to the literature. To provide an optimal depiction of gadolinium enhancement, a fat suppressed T1-TSE sequence was used.

We also examined areas of non irradiated bone marrow, as previous studies have reported that radiation-induced changes may occur outside the irradiation field. Blomlie et al. first observed

SI changes on T1W images in 58% of the patients and on STIR images in 48% in presumed "non-irradiated" areas [35]. Our results are in agreement with the literature.

The population used in this study was characterized by extremely poor physical status and relatively short life expectancy. The fact that we focused just on the early post-radiation lesions, allowed us to limit their follow-up time, without any significant impact on our results. Due to the above reason a relatively small number of patients were examined.

The alterations in the mean follow-up time intervals could be considered as another major limitation of our study, as these patients very often were suffering especially from pain and could not collaborate on the MR examination.

No histopathologic correlation was obtained for the lesions examined in this study, as this would be difficult, concerning the physical status of these patients. Without histologic correlation, it is difficult to fully explain the exact cause of the SI changes. However, the characterization of the lesions was based on the MRI changes, as well as to the image analysis system that we used, in accordance to the literature [16,17].

MRI can evaluate the degree of early therapy-induced bone marrow lesions observed during the first 18 days from the beginning of RT. The proposed neural network-based classification system might be used as an assisting tool for the characterization of these lesions.

References

1. Falkmer U, Järhult J, Wersäll P, Cavallin-Stahl E. A systemic overview of radiation therapy effects in skeletal metastases. Acta Oncol 2003; 42: 620-633.
2. Galasko CSB. The Anatomy and Pathways of Skeletal Metastases. In: Weiss I, Gilbert AH (Eds): Bone metastasis. GK Hall, Boston MA, 1981, pp 49-63.
3. Hoskin PJ. Scientific and clinical aspects of radiotherapy in the relief of bone pain. Cancer Surv 1988; 7: 69-86.
4. Chow E, Harris K, Fan G, Tsao M, Sze WMJ. Palliative radiotherapy trials for bone metastases. A systematic review. Clin Oncol 2007; 25: 1423-1436.
5. Sze WM, Shelley MD, Held I, Wilt TJ, Mason MD. Palliation of metastatic bone pain: single fraction versus multifraction radiotherapy. J Clin Oncol 2003; 15: 345-352.
6. Salazar OM, Sandhut T, da Motta MW et al. Fractionated half-body irradiation (HBI) for the rapid palliation of widespread, symptomatic, metastatic bone disease: a randomized phase III trial of the International Atomic Energy Agency (IAEA). Int J Radiat Oncol Biol Phys 2001; 50: 765-775.
7. Tong D, Gillick L, Hendrickson FR. The palliation of symptomatic osseous metastases: Final results of the Study by the Radiation Therapy Oncology Group. Cancer 1982; 50: 893–899.
8. Finlay IG, Mason MD, Shelley M. Radioisotopes for the palliation of metastatic bone cancer: a systematic review. Lancet Oncol 2005;6: 392-400.
9. Fertil, B, Melaise EP. Intrinsic radiosensitivity of human cell lines is correlated with radioresponsiveness of human tumors: analysis of 101 published survival curves. Int J Radiat Oncol Biol Phys1985; 11: 1699-1707.
10. Hoskin PJ. Bisphosphonates and radiation therapy for palliation of metastatic bone disease. Cancer Treat Rev 2003; 29: 321-327.
11. Hoskin PJ, Ford HT, Harmer CL. Hemibody irradiation (HBI) for metastatic bone pain in two histological distinct groups of patients. Clin Oncol 1989;1: 67-69.
12. Hoskin PJ, Stratford MRL, Folkes LK, Regan J, Yarnold JR. Effect of local radiotherapy for bone pain on urinary markers of osteoclast activity. Lancet Oncol 2000; 355: 1428-1429.
13. Vinholes JJ, Purohit OP, Abbey ME, Eastell R, Coleman RE. Relationships between biochemical and symptomatic response in a double-blind randomized trial of pamidronate for metastatic bone disease. Ann Oncol1997;8: 1243-1250.
14. Porter AT, Davis LP. Systemic radionuclide therapy of bone metastases with strontium-89. Oncology1994; 93–96; 99-101.
15. Remedios PA, Colletti PM, Raval JK et al. Magnetic resonance imaging of bone after radiation. Magn Reson Imaging 1988;6:301-304.
16. Stevens SK, Moore SG, Kaplan ID. Early and late bone marrow changes after irradiation: MR evaluation. AJR 1990;154:745-750.
17. Yankelevitz DF, Henshke CI, Knapp PH, Nisce L, Yi Y, Cahill P. Effect of radiation therapy on thoracic and lumbar bone marrow: Evaluation with MR imaging. AJR 1991; 157: 87-92.
18. Mitchell MJ, Logan PM. Radiation-induced changes in bone. Radiographics 1998; 18:1125-1136.
19. Daldrup – Link HE, Henning T, Link TM. MR imaging of therapy – induced changes of bone marrow. Eur Radiol 2007; 17: 743-761.
20. Hwang S, Panicek DM. Magnetic resonance imaging of bone marrow in oncology, Part 2. Skeletal Radiol 2007; 36: 1017-1027.
21. Otake S, Mayer N, Ueda T, Magnotta VA, Yuh WTC. Radiation-induced changes in MR signal intensity and contrast enhancement of lumbo-sacral vertebrae: Do changes occur only inside the radiation therapy

field? Radiology 2002; 222: 179-183.

22. Ramsey RG, Zacharias CE. MR imaging of the spine after radiation therapy: easily recognizable effects. Am J Neuroradiol 1985; 6: 247-251.
23. Ntoulia A, Papadopoulou F, Ristanis S, Argyropoulou M, Georgoulis AD. Revascularization Process of the Bone–Patellar Tendon–Bone Autograft Evaluated by Contrast-Enhanced Magnetic Resonance Imaging 6 and 12 Months After Anterior Cruciate Ligament Reconstruction. Am J Sports Med 2011; 39: 1478-1486.
24. Haralick RM, Shanmugam K, Dinstein I. Textural Features for Image Classification. IEEE Trans Syst Man Cybern 1973; SMC-3:610-621.
25. Galloway MM. Texture analysis using grey level run lengths. Comp Graph and Image Proc 1975; 4: 172-179.
26. Theodoridis S, Koutroumbas K. Pattern Recognition. Academic Press, New York, 1999.
27. Specht DF. Probabilistic Neural Networks. Neural Networks 1990; 3: 109-118.
28. Ahmed N, Rao R (Eds). Orthogonal Transforms for Digital Signal Processing. Springer-Verlag, NY, 1975.
29. Ambroise C, McLachlan GJ. Selection bias in gene extraction on the basis of microarray gene-expression data. Proc Natl Acad Sci USA 2002; 99: 6562-6566.
30. Vanel D. MRI of bone metastases: the choice of the sequence. Cancer imaging 2003; 4:30-35.
31. Olivier L, Gerber S, Vanel D, Brisse H, Leclere J. Improving the interpretation of bone marrow imaging in cancer patients. Cancer Imaging 2006; 6: 194-198.
32. Rubin P. Hematopoietic tissues and blood. In: Rubin P, Casarett GW (Eds): Clinical Radiation Pathology, Saunders, Philadelphia, vol. 2, pp 778-849.
33. Knopse WH, Blom J, Crosby WH. Regeneration of locally irradiated bone marrow. I. Dose dependent, long term changes in the rat, with particular emphasis upon vascular and stromal reaction. Blood 1966; 28: 398-415.
34. Sigimura H, Kisanuki A, Tamura S, Kihara Y, Watanabe K, Sumiyoshi A. Magnetic resonance imaging changes after irradiation. Invest Radiol 1994; 29: 35-41.
35. Blomlie V, Rofstad EK, Skonsberg A, Tvera K, Lien HH. Female pelvic bone marrow: serial MR imaging before, during and after radiation therapy. Radiology 1995; 194: 537-543.
36. Onu M, Savu M, Lungu-Solomonescu C, Harabagiu I, Pop T. Early MR changes in vertebral bone marrow for patients following radiotherapy. Eur Radiol 2001; 11: 1463-1469.
37. Biffar A, Baur-Melnyk A, Schmidt GP, Reiser MF, Dietrich O. Multiparameter MRI assessment of normal appearing and diseased vertebral bone marrow. Eur Radiol 2010; 20: 2679-2689.
38. Argiris A, Maris T, Papavasiliou G, Gouliamos A, Papavasiliou C. Radiotherapy effects on vertebral bone marrow: easily recognizable changes in T2 relaxation times. Magn Res Imag 1996; 14: 633-638.